INDIAN JOURNAL OF SCIENCE AND TECHNOLOGY

RESEARCH ARTICLE

MHD Boundary Layer Flow Past an Exponentially Stretching Sheet with Darcy-Forchheimer Flow of Nanofluids

Sonika Sharma[1]*

1 Research Scholar, Department of Mathematics and Statistics, Career Point University, Hamirpur (H.P), India

OPEN ACCESS

Received: 18-04-2022

Accepted: 25-07-2022

Published: 26.08.2022

Citation: Sharma S (2022) MHD Boundary Layer Flow Past an Exponentially Stretching Sheet with Darcy-Forchheimer Flow of Nanofluids. Indian Journal of Science and Technology 15(33): 1594-1604. https://doi.org/10.17485/IJST/v15i33.607

* **Corresponding author**.

sonikasharmablp@gmil.com

Funding: None

Competing Interests: None

Published By Indian Society for Education and Environment (iSee)

ISSN
Print: 0974-6846
Electronic: 0974-5645

Abstract

Objectives: To investigate an exponentially stretched sheet with a magnetic force to explore the Darcy-Forchheimer flow of a two-dimensional blood-based nanofluid and the effect of different relevant parameters of the fluid flow assumption for velocity and temperature profiles. **Methods**: Nanoparticles such as Ag, TiO_2 and Fe with base fluid blood are being investigated. The governing equations of the problem, such as continuity, motion, and energy, are derived and translated into ordinary differential equations by employing appropriate optimization techniques. The bvp4c technique is used to perform numerical computations. The impacts of non-dimensional governing factors like the prandtl number (Pr), magnetic field parameter (M), Forchheimer number (Fr), porosity parameter (β) and nanofluid volume fraction (ϕ) are determined numerically and displayed through graphs. Tables illustrate and explain the local Nusselt number and skin friction coefficient. **Findings**: Velocity profile of Ag-blood, TiO_2-blood and Fe-blood decreases and temperature profile increases for increasing values of Pr, β, M and Fr. For rising values of M, β, and Fr, the skin friction coefficient increases and the Nusselt number decreases, but the accelerating trend of ϕ exhibits a reversible trend. **Novelty**: The Darcy-Forchheimer flow of a two-dimensional blood-based nanofluid with a magnetic field is novel in the model. The (Ag-Blood, TiO_2-Blood, Fe-Blood) nanofluid flow past an exponentially stretching surface is considered in the present study, while no one has considered these nanofluids for the same model.

Keywords: MHD; Bloodbased nanofluid; Nanoparticles; Exponentially stretching surface; Darcy Forchheimer flow; Blood based nanofluid

1 Introduction

The investigation of boundary layer flow and thermal expansion over a stretching sheet has achieved remarkable success over the last decades, owing to the abundance of potential implementation in technology and industry. Some of them are the cooling of an endless metal plate into a cooling pot, the border layer along the conveyor of materials, the stream line along a liquid film in the form of condensation procedures,

the rolling of cable, paper production, heated rolling, glass processing, and plastic foil drawing. Crane [1] pioneered the flow of the boundary layer due to an extension plate that moved linearly from a fixed point with a varying speed. Over the past few years, numerous investigations have found that flow over a stretched sheet is caused by a linear fluctuation in the sheet's stretching rate. As a result, the limit layer flow impacted by an exponentially stretched sheet has not gotten much attention, despite the fact that this flow occurs often in many technical applications. Magyari and Keller [2] concentrated on the thermal transport in limit layer flow caused by an exponentially continuous stretch panel without fluctuating fluid properties and the application of magnetohydrodynamic (MHD). Heat transmission layout, catalytic reactor designs, geothermical systems, and geophysics are just a few of the applications in environmental and industrial systems for saturation of porous material. The flow of porous medium is extremely advantageous in a variety of applications, including fermentation, grain storage, groundwater contamination, reservoir movement, petroleum production, groundwater sources, fossil fuel systems, nuclear waste disposal, energy storage units, oil resources, solar panels, and many more. Darcy's [3] theory acted as a base for many studies related to porous media possessing low porosity and fluid velocities; nevertheless, it had limitations with media of high permeability and larger transportation. At high flow rates, the traditional Darcy's law fails to account for inertial and edge circumstances. That's why Darcy's theory was not applicable of giving an explanation of physical circumstances comprising high porosity media and velocities. As a workaround for this shortcoming, Forchheimer [4] introduced a square velocity component to the Darcy velocity model, which allowed for the determination of inertia and boundary characteristics. Wang et al. [5] explored two dimensional boundary layer flow of prandtl nanofluids in the presence of an aligned magnetic field over an inclined stretching/shrinking sheet in a non-Darcy permeable medium. Furthermore, they incorporated microorganisms to improve the stability of the base fluid and to avoid agglomeration of nanoparticles. Heat transfer coefficient measurements in nanofluids have yielded significant results in a variety of industrial processes. Nanofluids are a novel class of substances that contain nanoparticles suspended among a low thermal conductive traditional liquids like kerosene, water, or ethylene glycol. All such metal or metal oxide particles boost the conduction and convection coefficients, resulting in enhanced heat exchange from the cooling medium to the surrounding environment [6]. Human exposure to nanoparticles is inescapable because of their wide range of applications. In several studies, the lungs, digestive tract, liver, heart, spleen, kidneys, and cardiac muscle all accumulate nanoparticles after inhalation or oral exposure. Furthermore, they disrupt the equilibrium of glucose and lipids in rats and mice.

Generally, these nanoparticles usually include ceramics (Al_2O_3, CuO), metal nitrides (SiN,AlN), ferro particulates ($CoFe_2O_4$, Fe_3O_4, $Mn-ZnFe_2O_4$), metals (Cu,Ag, Au), carbohydrate in different formats (graphite, carbon nanotubes and diamonds) etc. Pushpa et al. [7] explored the buoyant convective flow and thermal transport augmentation of Cu– H_2O nanoliquid in a differentially heated upright annulus having a thin baffle. Swain et al. [8] studied the influence of variable magnetic fields and chemical reactions of $MWCNT/Fe_3O_4$-water on an exponentially porous shrinking sheet with slip boundary conditions. Pattnaik et al. [9] investigated heat transfer analysis on engine oil-based hybrid nanofluid past an exponentially stretching permeable surface with Cu/Al_2O_3 additives. Sharma and Sood [10] analyzed magneto hydrodynamics (MHD) boundary layer flow with heat and mass transfer of pseudo-plastic nanofluid over an exponentially stretching sheet embedded in a porous medium. Tiwari and Das [11] have created a single phase model with nanofluid properties as components of basic fluids and their components. The Tiwari and Das model, commonly known as the single phase model, focuses on the behavior of nanofluids while accounting for the nanofluid's solid volume fraction. Nanofluids composed of iron-based nanoparticles (also known as ferrofluids) are much effective as their heat transfer performance can be modified by applying a magnetic field. It has been shown that ferrofluids can be used in a number of medical applications, such as removing cancer tumors, enhancing magnetic resonance imaging (MRI), transferring heat through tissue, and reducing bleeding during surgery. Photo catalyst titanium dioxide (TiO2) is the most common because of its inexpensive cost, great oxidizing abilities, and ease of immobilization on a variety of surfaces. In overview, it has been noted that almost all tumor cells are destroyed by metal-TiO_2 nanocomposite particles rather than single TiO_2 nanoparticles, demonstrating the importance of using nano-materials in medicine. Using TiO2-based photo catalysts, Kanan et al. [12] look at recent advancements in the degradation of pesticides and other important organic contaminants in water sources. Because of its unique qualities,Ag can be used in a range of biomedical applications, which include permeability, strength, electrochemical properties, and anti-bacterial properties. Ag and Ag-related components have been used for anti-bacterial operations against a wide range of microorganisms, including microbes, protozoa, fungi, and even the most recent viruses. Their contributions demonstrate that Ag particles have an anti-tumor effect. These particles could be a more cost-effective cancer treatment than other treatments. [13] In terms of surface area to volume ratio, magnetic nanoparticles are ideal for drug delivery because of their high substitution levels. Iron nanoparticles may oxidize and decrease numerous contaminants, unlike standard absorbents. Iron nanoparticles remove organic and inorganic contaminants from polluted water, soil, and sediments. Additionally, their biocompatibility and potential medical uses are enhanced by their ability to be included into composites such as magnetic hydrogels or liposomes. [14]

Intrigued by the forgoing findings and their ever increasing applications in various fields such as biomedical sciences, chemical processes, engineering and industrial sectors, we have set a goal to explore the boundary layer flow of an exponentially extended sheet with blood-based nanofluid. To the extent of our knowledge, no attempts have been made for such research as of yet. Therefore, we consider the flow, which is primarily made up of three types of nanoparticles: Ag, TiO_2, and Fe with blood as the base fluid. The one-phase model (Tiwari-Das model) is used in this study. In order to solve the controlling partial differential equations, similarity transformations are used to convert them into a set of ordinary differential equations, which are then numerically solved using the bvp4c method. The obtained findings are analyzed through tables and figures.

2 Methodology

A steady stream line flow and heat transfer properties of nanofluids over an exponentially extending sheet incorporated in porous media with MHD phenomenon is taken into account. The porous medium is explained using the Darcy Forchheimer model. It should be noted that the x-axis is parallel to the enlarged surface, whereas the y-axis is opposite to it. The stretching velocity at the free stream is of the form $U_w = U_0 e^{x/l}$. It is supposed that a magnetic field $B(x)$ is enforced on the surface in the normal direction. T_w is temperature at wall and T_∞ represents temperature of the surrounding environment. It is presumable that the base fluid and the nanoparticles are in a state of thermal equilibrium with one another and that there is no slip between them, and by adding surfactant we can avoid agglomeration of nanoparticles. Figure 1 depicts the flow geometry of the present study. The boundary layer conservation equations for mass, momentum, and energy are[15] :

$$\frac{\partial u}{\partial x} + \frac{\partial v}{\partial y} = 0 \qquad (1)$$

$$u\frac{\partial u}{\partial x} + v\frac{\partial u}{\partial y} = \frac{\mu_{nf}}{\rho nf}\left(\frac{\partial^2 u}{\partial y^2}\right) - \frac{\sigma B^2}{\rho_{nf}}u - \frac{\nu_{nf}}{K}u - \frac{F}{\rho_{nf}}u^2 \qquad (2)$$

$$u\frac{\partial T}{\partial x} + v\frac{\partial T}{\partial y} = \alpha_{nf}\left(\frac{\partial^2 T}{\partial y^2}\right) \qquad (3)$$

u and v represent the velocities in x and y directions, respectively. K is permeability of the porous medium and $F = \frac{c_b}{\sqrt{\lambda}L}$ is the non-uniform inertia coefficient of porous medium, where c_b is the form of drag coefficient dependent on geometry of the medium. $\nu_{nf} = \frac{\mu_{nf}}{\rho_{nf}}$ denotes the kinematic viscosity of nanofluid where μ_{nf} is the viscosity of nanofluid and ρ_{nf} is the density of nanofluid. T denotes temperature, κ_{nf} denotes the thermal conductivity of nanofluid and specific heat capacity by $(\rho c_p)_{nf}$.

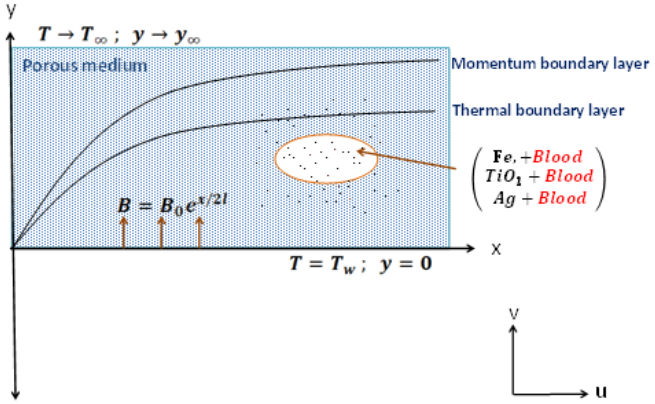

Fig 1. The diagram depicting the problem's flow

Table 1. Thermophysical properties of nanofluid [16,17]

Properties	Nanofluid
Density	$\rho_{nf} = (1-\phi)\rho_f + \phi\rho_s$
Heat Capacity	$(\rho c_p)_{nf} = (1-\phi)(\rho c_p)_f + \phi(\rho c_p)_s$
Thermal Conductivity	$\frac{\kappa_{nf}}{\kappa_f} = \frac{(\kappa_S+2\kappa_f)-2\phi(\kappa_f-\kappa_S)}{(\kappa_S+2\kappa_f)+\phi(\kappa_f-\kappa_S)}$
Dynamic Viscosity	$\mu_{nf} = \frac{\mu_f}{(1-\phi)^{2.5}}$

To derive similarity solutions, the magnetic field B(x) is assumed to have the form

$$B = B_0 e^{(x/2l)} \tag{4}$$

where B_0 symbolizes a magnetic field that is constant. The given problem has the following boundary conditions:

$$\begin{gathered}\{u = U_w(x) = Ue^{x/l},\ v = 0,\}\ at\ y = 0,\\ u \to 0,\ T \to T_\infty,\ as\ y \to \infty\end{gathered} \tag{5}$$

$T_w = T_\infty + T_0 e^{x/2l}$, wall temperature, is assumed constant at the stretching sheet. T is fluid's temperature, U is the velocity component and T_0 is the temperature component in the stretching sheet. Using the following similarity transformations

$$\eta = \sqrt{\frac{U}{2\nu_f l}}\, e^{x/2l} y,\ u = Ue^{x/l} f',\ v = -\sqrt{\frac{\nu_f U}{2l}} e^{x/2l}(f + \eta f'), \theta = \frac{T-T_\infty}{T_w - T_\infty}, \tag{6}$$

Substituting eq.(10) in eqs. (2) and (3), the following non-linear ordinary differential equations are derived:

$$f''' - \left(\frac{\rho_{nf}/\rho_f}{\mu_{nf}/\mu_f}\right)\left(2f'^2 + ff''\right) - (1-\phi)^{2.5} Mf' - \beta f' - (1-\phi)^{2.5} Frf'^2 = 0 \tag{7}$$

$$\frac{1}{Pr}\left(\frac{\kappa_{nf}/\kappa_f}{(\rho c_p)_{nf}/(\rho c_p)_f}\right)\theta'' - f'\theta + f\theta' = 0 \tag{8}$$

where $Pr = \mu_f/\alpha_f$, $M = \frac{2\sigma B_0^2 l}{\rho_f U}$, $\beta = \frac{2\nu_f l}{KU_w}$, and Fr = $\frac{2Fl}{\rho_f}$ .The modified boundary conditions are as follows:

$$\begin{gathered}f = 0, f' = 1, \theta = 1\ at\ \eta = 0\\ f' \to 0,\ \theta \to 0\ as\ \eta \to \infty\end{gathered} \tag{9}$$

The physical parameters of relevance, the skin friction coefficient C_f and local Nusselt number Nu_x, are derived as:

$$C_{fx} = \frac{\tau_w}{\rho_f U^2}\ and\ Nu_x = \frac{xq_w}{\kappa_f(T_w - T_\infty)} \tag{10}$$

where $\tau_w = \mu_{nf}\left(\frac{\partial u}{\partial y}\right)_{y=0}$ is the shear stress and $q_w = -\kappa_{nf}\left(\frac{\partial T}{\partial y}\right)_{y=0}$ is the heat transfer rate of surface. Using similarity transformations (10) in above equations, we obtain

$$\sqrt{2Re_x}\, C_{fx} = \frac{1}{(1-\phi)^{2.5}} f''(0),\ Re_x^{-1/2} Nu_x = -\frac{\kappa_{nf}}{\kappa_f}\sqrt{\frac{x}{2l}}\theta'(0) \tag{11}$$

where $Re_x = \frac{Ue^{x/l}}{\nu_f}$ is the local Reynold number.

2.1 Numerical Technique: bvp4c solver

According to Hale [18], Kierzenka and Shampine [19] were responsible for developing and implementing the bvp4c solver. They established the bvp4c solver, which allows them to figure out the border line problem for a coupled nonlinear ordinary differential equation in a more straightforward manner than before. The program is a finite-differential code that solves the system of equations using the three-stage Labatto IIIa formula and its algorithm, which is based on an iteration structure.

Utilizing non-dimensional parameters, we reduce the controlling partial differential equations (2) and (3) to non-linear ordinary differential equations (7) and (8), which we then solve with the boundary value problem solver bvp4c in MATLAB. The purpose of simplifying ordinary differential equations is to make them easier to solve numerically. This section will go into detail about how the bvp4c is implemented for the current problem. In steps 1 and 2, we explored how to convert the structure of ordinary differential equations for the current situation to a framework of five first order equations. The boundary condition is converted in step 3 and the rest of the program is completed in step 4.

Step 1: Above all, we will introduce additional variables into Eqs. (7), (8), and (9) for the paired nonlinear ODEs:

$$f = y(1), f^{'} = y(2), f^{''} = y(3)$$
$$\theta = y(4), \theta^{'} = y(5),$$

Step 2: In this step, we will write these factors in the first order system of equations as shown:

$$f^{'} = y(2), f^{''} = y(3),$$
$$f''' = \frac{\rho_{nf}/\rho_f}{\mu_{nf}/\mu_f}\left(2\,y(2)^2 - y(1)\,y(3)\right] + \beta\,y(2) + (1-\phi)^{2.5} Fr\,y(2)^2 + (1-\phi)^{2.5} M\,y(2)$$
$$\theta = y(4), \theta' = y(5),$$
$$\theta'' = Pr\,\frac{(\rho c_p)_{nf}/(\rho c_p)_f}{\kappa_{nf}/\kappa_f}\,(y(2)\,y(4) - y(1)\,y(5)]$$

Step 3: In accordance with the new variables, the boundary conditions are transformed into:

$$ya(1) = 0,\ ya(2) = 1,\ ya(4) = 1,\ yb(2) = 0,\ yb(4) = 0$$

Step 4: We explain the system of first order equations with boundary conditions utilizing bvp4c solver in MATLAB software.

3 Result and Discussion

This segment deals with the description of impact of the all the governing flow parameter on the flow variable i.e. velocity and temperature. Using the bvp4c technique, we solve differential equations (7) and (8) subject to conditions (9). In this section, the effects of essential parameter on speed and temperature profiles are studied very closely with the help of graphs and computational results. Various forms of nanofluids, namely Ag-Blood, TiO_2-Blood and Fe-Blood have been studied with prandtl number Pr, magnetic field parameter M, porosity parameter β, forchhiemer number Fr and nanoparticle volume fraction ϕ. To ensure that our findings are correct, we compared them to those of previous studies. Table 2 demonstrates a comprehensive analysis of values of $-\theta'(0)$ for Cu-water based nanofluids for numerous values of Pr in a manner that $M = \beta = Fr = \phi = 0$ and the results acquired are validated with the results of Magyari and keller[2], El. Aziz[20] and Loganathan and Vimala[21]. The values obtained in this study are consistent, and thus we are confident in the accuracy of our findings.

Table 2. Comparative analysis of results obtained for the temperature gradient

Pr	Magyari and keller	El. Aziz	Loganathan and Vimla	Present Study
1	0.954782	0.954785	0.955870	0.954788
3	1.869075	1.869074	1.868878	1.869073
5	2.500135	2.500132	2.499982	2.5001213
10	3.660379	3.660372	3.660239	3.660289

ists the thermo physical characteristics of the conventional fluid (blood) as well as the nanoparticles. Table 4 and Table 5 displayed the skin friction coefficient and local Nusselt number with reference to M, β, Fr and ϕ. It is noticed that the skin friction coefficient demonstrate increasing behavior for rising values of magnetic field parameter M, porosity parameter β and Forchhiemer number in case of all three nanofluids Ag-Blood, TiO_2-Blood and Fe-Blood and shows opposite behaviour for Nusselt number. However skin friction factor reduces and Nusselt number grows with increasing values of nanoparticle volume fraction ϕ for Ag-Blood and increasing in case of TiO_2-Blood and Fe-Blood.

The numerical calculations have been done by setting the values of the parameters as $Pr = 25$, $\beta = 0.3$, $Fr = 0.4$, $M = 1$, and $\phi = 0.1$, if not defined otherwise. The Figure 2 illustrates the effect of various values of prandtl number Pr on the temperature component $\theta(\eta)$ for all three nanofluids Ag-Blood, TiO_2-Blood, and Fe-Blood with base fluid blood. As demonstrated in the figure, enhancing the prandtl number Pr results in a decline in the thermal boundary layer. This is due to the fact that increasing Pr makes the kinematic viscosity go up while the thermal conductivity goes down. This result shows a very good match with[24].

Table 3. Thermophysical properties of Blood and considering nanoparticles [22,23] :

Base fluid and nanoparticles	$\rho(kg/m^3)$	$c_p(J/kgK)$	$\kappa(W/mK)$
Blood	1050	3617	0.52
Silver (Ag)	10500	235	429
Titania (TiO_2)	4250	686.5	8.95
Iron (Fe)	7870	460	80

Figure 3 and Figure 4 show that how the magnetic field factor M changes flow speed and temperature. When M is increased, the fluid velocity demonstrated in Fig. 3 depicts that the flow rate decreases significantly. Physically, as the Lorentz force rises with the magnetic factor, this demonstrates that the longitudinal magnetic field resists fluid flow. We can see from Figure 4 that as the magnetic flux enhanced, so did the temperature of the fluid. A frictional resistive force called the Lorentz force is responsible for this. This is because the thickness of the temperature field boosts the magnetic field's strength. Figure 5 amplifies the influence of the porosity parameter β on $f'(\eta)$. The velocity field parameter $f'(\eta)$ decreases as the porosity parameter β increases. Physically, with an increase in β the porous space also increases, which causes friction in the fluid stream and diminishes the flow motion of nanoparticles. Due to the increased viscosity of the thermal boundary layers, the porous surface has a significant effect on their development. Increased porosity results in decreased permeability. Due to this $f'(\eta)$ and momentum boundary layer declines. As shown in Figure 6 the porosity parameter β changes in relation to the temperature profile $\theta(\eta)$ for three different nanoparticles: silver, titanium dioxide, and iron oxide. Having porous media increases the resistance to flow and consequently raises the temperature of the fluid. The results obtained in this study for M and β have well agreement with [25]. The influences of Ag, TiO_2 and Fe nanoparticle concentration ϕ with base fluid blood on velocity field $f'(\eta)$ is depicted pictorially in Figure 7. The velocity distribution $f'(\eta)$ declined in comparison to the rising volume fraction of nanoparticles. This signifies that when nanoparticle concentration goes up, the flow slows down and the thickness of momentum boundary layer goes up. The impact of nanoparticle concentration ϕ on the thermal distribution $\theta(\eta)$ in case of Ag-Blood, TiO_2-Blood and Fe-Blood is portrayed in Figure 8. Physically, when the value of ϕ rises, the temperature profile rises, which is caused by the collision of the suspended nanoparticles. Physically, when nanoparticles are added, thermal conductivity rises, and the thickness of the temperature field rises as well [26]. Figure 9 depicts the deviation in velocity distribution $f'(\eta)$ for differing Forchhiemer number Fr. The velocity distribution $f'(\eta)$ moves more slowly as the Forchhiemer value Fr rises. In a nutshell, the higher the inertial coefficient, the more resistance there is in the fluid path, which makes it easier for nanofluid to move. Figure 10 describe the behavior of Forchhiemer number Fr on temperature profile $\theta(\eta)$. In order to increment in Fr, the temperature distribution $\theta(\eta)$ of all Ag-Blood, TiO_2-Blood and Fe-Blood is significantly accelerated. This result is consent to the work done by [26].

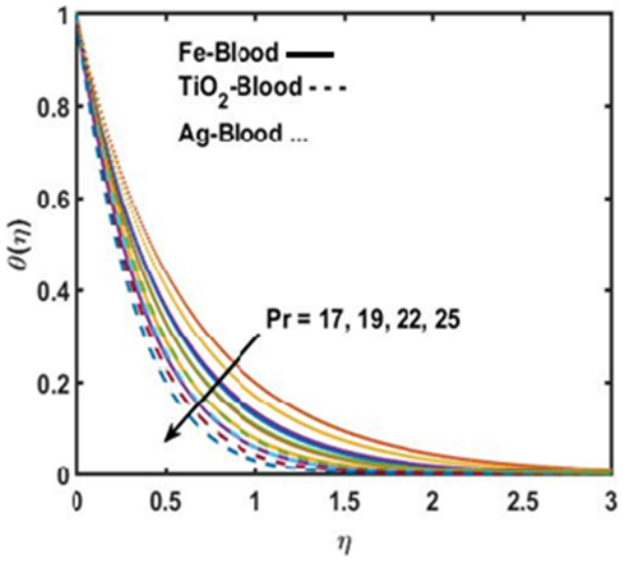

Fig 2. The thermal distribution $\theta(\eta)$ of Fe-Blood, TiO2-Blood and Ag-Blood for deviating values of Pr

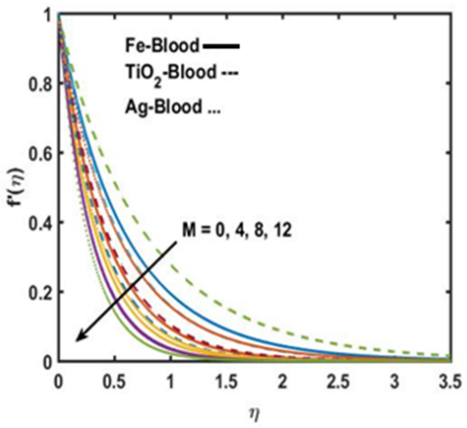

Fig 3. The velocity distribution $f'(\eta)$ of Fe -Blood, TiO2-Blood and Ag-Blood for deviating values of M

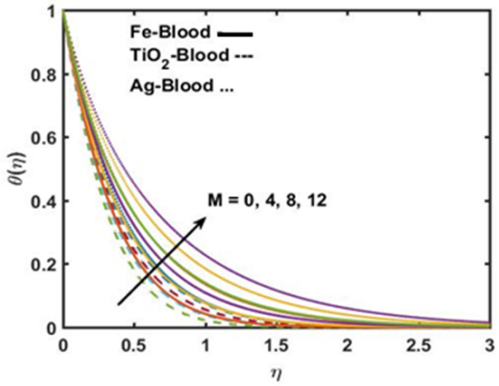

Fig 4. The thermal distribution $\theta(\eta)$ of Fe-Blood, TiO2-Blood and Ag-Blood for deviating values of M

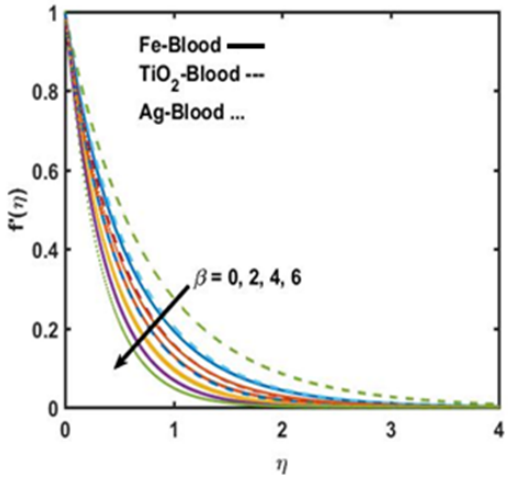

Fig 5. The velocity distribution $f'(\eta)$ of Fe -Blood, TiO2-Blood and Ag-Blood for deviating values of β

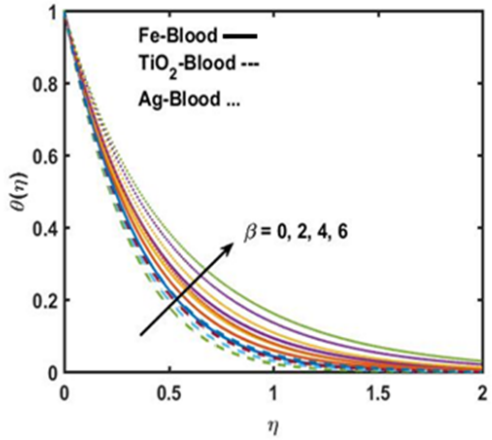

Fig 6. The thermal distribution $\theta(\eta)$ of Fe-Blood, TiO2-Blood and Ag-Blood for deviating values of β

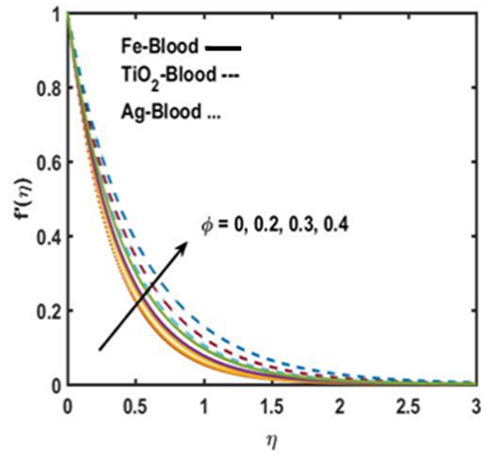

Fig 7. The velocity distribution $f'(\eta)$ of Fe -Blood, TiO2-Blood and Ag-Blood for deviating values of φ

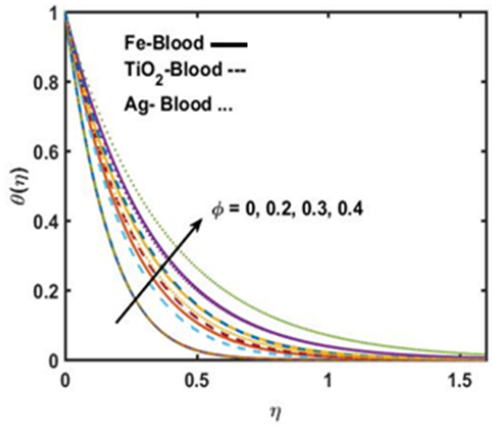

Fig 8. The thermal distribution $\theta(\eta)$ of Fe-Blood, TiO2-Blood and Ag-Blood for deviating values of φ

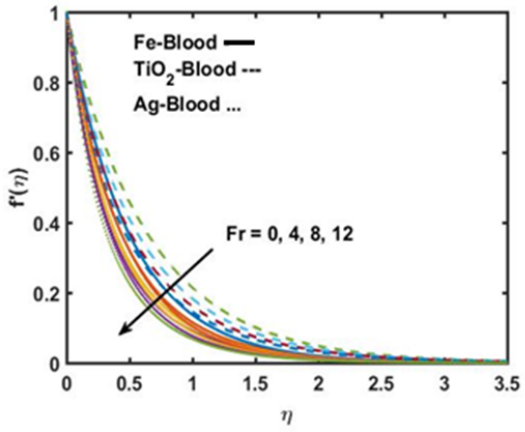

Fig 9. The velocity distribution $f'(\eta)$ of Fe -Blood, TiO2-Blood and Ag-Blood for deviating values of Fr

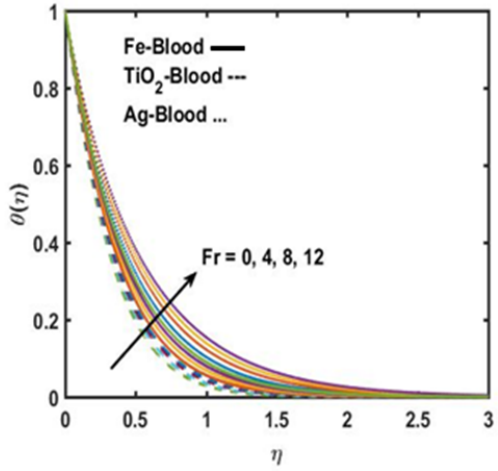

Fig 10. The thermal distribution $\theta(\eta)$ of Fe-Blood, TiO2-Blood and Ag-Blood for deviating values of Fr

Table 4. Numerical analysis of the current study for skin friction coefficient $\frac{1}{(1-\phi)^{2.5}} f''(0)$ when $Pr = 25$.

M	β	Fr	ϕ	$-\frac{1}{(1-\phi)^{2.5}} f''(0)$ for (Ag-blood)	$-\frac{1}{(1-\phi)^{2.5}} f''(0)$ for (TiO_2-blood)	$-\frac{1}{(1-\phi)^{2.5}} f''(0)$ for (Fe-blood)
0.5	0.3	0.4	0.1	0.34539	0.30346	0.32841
0.8	0.3	0.4	0.1	0.34779	0.306190	0.33093
1.0	0.3	0.4	0.1	0.34938	0.30799	0.33260
1.5	0.3	0.4	0.1	0.35332	0.31244	0.33673
1.0	0.1	0.4	0.1	0.26064	0.20221	0.23782
1.0	0.3	0.4	0.1	0.27247	0.21717	0.25070
1.0	0.5	0.4	0.1	0.28379	0.23116	0.26294
1.0	1.0	0.4	0.1	0.31044	0.26286	029126
1.0	0.3	0.1	0.1	0.35259	0.31159	0.33596
1.0	0.3	0.2	0.1	0.35311	0.31218	0.33650
1.0	0.3	0.3	0.1	0.35362	0.31276	0.33705
1.0	0.3	0.4	0.1	0.35414	0.31235	0.33759
1.0	0.3	0.4	0	2.51467	2.51467	2.51467

Continued on next page

Table 4 continued

1.0	0.3	0.4	0.1	1.95410	1.83631	1.90543
1.0	0.3	0.4	0.2	1.42303	1.28682	1.36741
1.0	0.3	0.4	0.3	0.97056	0.85942	0.92545

Table 5. Numerical analyses of the current study for Nusslet number

M	β	Fr	ϕ	$-\frac{\kappa_{nf}}{\kappa_f}\theta'(0)$ for (Ag-blood)	$-\frac{\kappa_{nf}}{\kappa_f}\theta'(0)$ for (TiO_2-blood)	$-\frac{\kappa_{nf}}{\kappa_f}\theta'(0)$ for (Fe-blood)
0.5	0.3	0.4	0.1	9.45501	9.18443	10.44742
0.8	0.3	0.4	0.1	9.44070	9.17168	10.43289
1.0	0.3	0.4	0.1	9.43120	9.16324	10.42327
1.5	0.3	0.4	0.1	9.40765	9.14235	10.39939
1.0	0.1	0.4	0.1	9.95729	9.65228	10.96450
1.0	0.3	0.4	0.1	9.88772	9.58400	10.89167
1.0	0.5	0.4	0.1	9.82096	9.51988	10.82227
1.0	1.0	0.4	0.1	9.66434	9.37359	10.66085
1.0	0.3	0.1	0.1	9.40390	9.14070	10.39662
1.0	0.3	0.2	0.1	9.40174	9.13858	10.39428
1.0	0.3	0.3	0.1	9.39953	9.13645	10.39196
1.0	0.3	0.4	0.1	9.39735	9.13434	10.38964
1.0	0.3	0.4	0	5.66011	5.660112	5.66011
1.0	0.3	0.4	0.1	6.28707	6.26046	6.40585
1.0	0.3	0.4	0.2	6.93693	6.88657	7.20801
1. 0	0.3	0.4	0.3	7.64192	7.5736	8.10323

4 Conclusion

The Darcy-Forchheimer and MHD boundary layer flows past an exponentially stretched sheet are examined in detail in this work and compared to previously published results. The impact of varying the nanoparticle volume fraction on two-dimensional boundary layer flow has been examined in this study. Hepatic cirrhosis, heart failure, cardiomyopathy, conduction abnormalities, and diabetes mellitus are all long-term side effects of iron excess from transfusions. Small doses of TiO_2 nanoparticles can influence the intestinal mucosa, brain, heart, and other internal organs, increasing the risk of many diseases, tumors, or the progression of current cancer procedures. In the future, Ag, TiO_2 and Fe synthesis, which is advanced and good for the environment, could be a good replacement for traditional physical and chemical methods. The effects of Ag, TiO_2, and Fe are accounted for by employing homogeneous flow model. The main findings of this study are:

1. Velocity profile of Ag-blood, TiO_2-blood and Fe-blood decreases for increasing values of Pr, β, M and Fr but opposite trend for ϕ.
2. Temperature profile of iAgblood, iTiO_2blood and iFeblood increases for increasing values of Pr, β, M, Fr and Φ.
3. For greater values of M, β, and Fr, the skin friction coefficient increases and the Nusselt number decreases, whereas the contrary tendency is found for increasing ϕ.

References

1) Crane LJ. Flow past a stretching plate. *Zeitschrift für angewandte Mathematik und Physik ZAMP*. 1970;21(4):645–647. Available from: https://doi.org/10.1007/BF01587695.
2) Magyari E, Keller B. Heat and mass transfer in the boundary layers on an exponentially stretching continuous surface. *Journal of Physics D: Applied Physics*. 1999;32(5):577–585. Available from: https://doi.org/10.1088/0022-3727/32/5/012.
3) Darcy H. Les fontaines publiques de la ville de Dijon: exposition et application... Victor Dalmont. 1856.
4) and PF. Wasserbewegung durch boden. Z. Ver. Deutsch, Ing. 1901.

5) Wang J, Mustafa Z, Siddique I, Ajmal M, Jaradat MMM, Rehman SU, et al. Computational Analysis for Bioconvection of Microorganisms in Prandtl Nanofluid Darcy–Forchheimer Flow across an Inclined Sheet. *Nanomaterials*. 2022;12(11):1791–1791. Available from: https://doi.org/10.3390/nano12111791.
6) Choi SU, Eastman JA. Enhancing thermal conductivity of fluids with nanoparticles. *Argonne National Lab (ANL)*. 1995.
7) Pushpa BV, Sankar M, Mebarek-Oudina F. Buoyant Convective Flow and Heat Dissipation of Cu–H₂O Nanoliquids in an Annulus Through a Thin Baffle. *Journal of Nanofluids*. 2021;10(2):292–304. Available from: https://doi.org/10.1166/jon.2021.1782.
8) Swain K, Mebarek-Oudina F, Abo-Dahab SM. Influence of MWCNT/Fe3O4 hybrid nanoparticles on an exponentially porous shrinking sheet with chemical reaction and slip boundary conditions. *Journal of Thermal Analysis and Calorimetry*. 2022;147(2):1561–1570. Available from: https://doi.org/10.1007/s10973-020-10432-4.
9) Pattnaik PK, Mishra S, Baag S. Heat transfer analysis on Engine oil-based hybrid nanofluid past an exponentially stretching permeable surface with Cu/Al₂O₃ additives. *Proceedings of the Institution of Mechanical Engineers, Part N: Journal of Nanomaterials, Nanoengineering and Nanosystems*. 2022;p. 239779142210938–239779142210938. Available from: https://doi.org/10.1177/23977914221093846.
10) Sharma D, Sood S. Effect of inclined magnetic field on flow of Williamson nanofluid over an exponentially stretching surface in Darcy-Forchheimer model. *ZAMM - Journal of Applied Mathematics and Mechanics / Zeitschrift für Angewandte Mathematik und Mechanik*. 2022;102(6). Available from: https://doi.org/10.1002/zamm.202100425.
11) Tiwari RK, Das MK. Heat transfer augmentation in a two-sided lid-driven differentially heated square cavity utilizing nanofluids. *International Journal of Heat and Mass Transfer*. 2007;50(9-10):2002–2018. Available from: https://doi.org/10.1016/j.ijheatmasstransfer.2006.09.034.
12) Kanan S, Moyet MA, Arthur RB, Patterson HH. Recent advances on TiO₂-based photocatalysts toward the degradation of pesticides and major organic pollutants from water bodies. *Catalysis Reviews*. 2020;62(1):1–65. Available from: https://doi.org/10.1080/01614940.2019.1613323.
13) Dawadi S, Katuwal S, Gupta A, Lamichhane U, Thapa R, Jaisi S, et al. Current Research on Silver Nanoparticles: Synthesis, Characterization, and Applications. *Journal of Nanomaterials*. 2021;2021:1–23. Available from: https://doi.org/10.1155/2021/6687290.
14) Schneider M, Martín MG, Otarola MJ, Vakarelska J, Simeonov E, Lassalle V, et al. Biomedical Applications of Iron Oxide Nanoparticles: Current Insights Progress and Perspectives. *Pharmaceutics*. 2022;14(1). Available from: https://doi.org/10.3390/pharmaceutics14010204.
15) Ghosh S, Mukhopadhyay S. Effects of slip on Cu–water or Fe $$_{3}$$ 3 O $$_{4}$$ 4 –water nanofluid flow over an exponentially stretched sheet. *Pramana*. 2019;92(6). Available from: https://doi.org/10.1007/s12043-019-1754-y.
16) Brinkman HC. The viscosity of concentrated suspensions and solutions. *The Journal of chemical physics*. 1952;20. Available from: https://doi.org/10.1063/1.1700493.
17) Khanafer K, Vafai K, Lightstone M. Buoyancy-driven heat transfer enhancement in a two-dimensional enclosure utilizing nanofluids. *International journal of heat and mass transfer*. 2003;46:3639–53. Available from: https://doi.org/10.1016/S0017-9310(03)00156-X.
18) Hale NP. A sixth-order extension to the matlab bvp4c software of j. kierzenka and l. shampine. Department of Mathematics. Imperial College London. 2006.
19) Kierzenka J, Shampine LF. A BVP solver based on residual control and the Maltab PSE. *ACM Transactions on Mathematical Software*. 2001;27(3):299–316. Available from: https://doi.org/10.1145/502800.502801.
20) El-Aziz MA. Viscous dissipation effect on mixed convection flow of a micropolar fluid over an exponentially stretching sheet. *Canadian Journal of Physics*. 2009;87(4). Available from: https://doi.org/10.1139/P09-047.
21) Loganathan P, Vimala C. MHD Boundary Layer Flow of a Nanofluid Over an Exponentially Stretching Sheet in the Presence of Radiation. *Heat Transfer-Asian Research*. 2014;43(4):321–331. Available from: https://doi.org/10.1002/htj.21077.
22) Srinivas S, Vijayalakshmi A, Reddy AS. Flow and Heat Transfer of Gold-Blood Nanofluid in a Porous Channel with Moving/Stationary Walls. *Journal of Mechanics*. 2017;33(3):395–404. Available from: https://doi.org/10.1017/jmech.2016.102.
23) Mushtaq A, Mustafa M, Hayat T, Alsaedi A. Numerical study for rotating flow of nanofluids caused by an exponentially stretching sheet. *Advanced Powder Technology*. 2016;27(5):2223–2231. Available from: https://doi.org/10.1016/j.apt.2016.08.007.
24) Jafar AB, Shafie S, Ullah I. MHD radiative nanofluid flow induced by a nonlinear stretching sheet in a porous medium. *Heliyon*. 2020;6(6):e04201–e04201. Available from: https://doi.org/10.1016/j.heliyon.2020.e04201.
25) Sharma S. Study on Darcy-Forchheimer Flow and MHD Boundary Layer Flow with Heat Transfer Characteristics of Williamson Nanofluid Over Curved Stretching Surface. *Journal of Physics: Conference Series*. 2021;1979(1):012046–012046. Available from: https://doi.org/10.1088/1742-6596/1979/1/012046.
26) Chandel S, Sood S. Unsteady flow of Williamson fluid under the impact of prescribed surface temperature (PST) and prescribed heat flux (PHF) heating conditions over a stretching surface in a porous enclosure. *ZAMM - Journal of Applied Mathematics and Mechanics / Zeitschrift für Angewandte Mathematik und Mechanik*. 2022;102(3). Available from: https://doi.org/10.1002/zamm.202100128.